**Atmospheric
Chemistry
and Physics**
Discussions

Open Access

Effect of chemical structure on secondary organic aerosol formation from C_{12} alkanes

L. D. Yee[1], J. S. Craven[2], C. L. Loza[2], K. A. Schilling[2], N. L. Ng[3],
M. R. Canagaratna[4], P. J. Ziemann[5], R. C. Flagan[2,1], and J. H. Seinfeld[2,1]

[1]Division of Engineering and Applied Science, California Institute of Technology, Pasadena, CA, USA
[2]Division of Chemistry and Chemical Engineering, California Institute of Technology, Pasadena, CA, USA
[3]School of Chemical and Biomolecular Engineering and School of Earth and Atmospheric Sciences, Georgia Institute of Technology, Atlanta, Georgia, USA
[4]Aerodyne Research, Inc., Billerica, Massachussets, USA
[5]Air Pollution Research Center, Department of Environmental Sciences, and Environmental Toxicology Graduate Program, University of California, Riverside, California, USA

Correspondence to: J. H. Seinfeld (seinfeld@caltech.edu)

Discussion Paper | Discussion Paper | Discussion Paper | Discussion Paper

ACPD

13, 10859–10903, 2013

Effect of chemical structure on SOA formation

L. D. Yee et al.

Title Page

Abstract	Introduction
Conclusions	References
Tables	Figures

|◄ | ►|
◄ | ►

Back | Close

Full Screen / Esc

Printer-friendly Version

Interactive Discussion

Title Page

Abstract | Introduction

Conclusions | References

Tables | Figures

|◄ | ►|

◄ | ►

Back | Close

Full Screen / Esc

Printer-friendly Version

Interactive Discussion

Abstract

The SOA formation from four C_{12} alkanes (*n*-dodecane, 2-methylundecane, hexylcyclohexane, and cyclododecane) is studied in the Caltech Environmental Chamber under low-NO_x conditions, in which the principal fate of the peroxy radical formed in the initial
5 OH reaction is reaction with HO_2. Simultaneous gas- and particle-phase measurements elucidate the effect of alkane structure on the chemical mechanisms underlying SOA growth. Reaction of branched structures leads to fragmentation and more volatile products, while cyclic structures are subject to faster oxidation and lead to less volatile products. Product identifications reveal that particle-phase reactions involving peroxy-
10 hemiacetal formation from several multi-functional hydroperoxide species initiate SOA growth in all four systems. The continued chemical evolution of the particle-phase is structure-dependent, with 2-methylundecane SOA formation exhibiting the least extent of chemical processing and cyclododecane SOA achieving sustained growth with the greatest variety of chemical pathways. The extent of chemical development is not nec-
15 essarily reflected in the oxygen to carbon (O:C) ratio of the aerosol as cyclododecane achieves the lowest O:C, just above 0.2, by the end of the experiment and hexylcyclohexane the highest, approaching 0.35.

1 Introduction

Long-chain alkanes constitute a significant component of the unresolved complex mix-
20 ture (UCM) in motor vehicle fuel sources and its combustion products (Schauer et al., 1999, 2002) and are a potential source of atmospheric secondary organic aerosol (SOA) formation (Robinson et al., 2007). However, the extent of SOA formation from atmospheric alkane photooxidation remains uncertain (Bahreini et al., 2012; Gentner et al., 2012). Each fuel type (e.g. gasoline vs. diesel) has different distributions of alkane
25 chain length and structure in terms of straight-chain, branched, cyclic, and cyclic + branched conformations (Schauer et al., 1999, 2002; Isaacman et al., 2012; Gentner

et al., 2012). This variety in structure leads to chemical differences in the processes leading to SOA formation, which have been the subject of extensive laboratory studies (Lim and Ziemann, 2005; Lipsky and Robinson, 2006; Lim and Ziemann, 2009a,b,c; Presto et al., 2009, 2010; Nakao et al., 2011; Lambe et al., 2012; Tkacik et al., 2012) and modeling efforts (Jordan et al., 2008; Pye and Pouliot, 2012; Zhang and Seinfeld, 2012; Aumont et al., 2012; Cappa et al., 2013).

Gas-phase chemical mechanisms for the OH-initiated oxidation of alkanes in the presence of NO_x have been studied (Atkinson, 1994, 1997; Atkinson and Arey, 2003; Atkinson et al., 2008). Many aspects of key particle-phase reactions for these species have also been explored (Aschmann et al., 2003; Dibble, 2007; Lim and Ziemann, 2009c). The prevailing level of NO_x is fundamental in atmospheric oxidation chemistry, as it controls, among other steps, the fate of the alkyl peroxy radical (RO_2) formed in the initial OH-organic reaction. The designation, high- and low-NO_x, refer to conditions in which the RO_2 fate is predominantly RO_2 + NO and RO_2 + HO_2, respectively. These cases represent idealizations of actual atmospheric conditions, but they allow isolation of the mechanistic pathways leading to SOA formation in the two cases.

We focus here on the low-NO_x oxidation mechanisms of four C_{12} alkanes (*n*-dodecane, 2-methylundecane, hexylcyclohexane, and cyclododecane) (Table 1). The C_{12} alkane system is a prototype for relatively long alkanes, which are characterized by side chains and cyclic structure in addition to a linear structure. The distribution of oxidation products comprise a variety of functionalizations (hydroperoxy, hydroxyl, ketone, aldehyde, carboxylic acid, and peracid). Detailed study of the C_{12} system affords insight into the effect of alkane structure on SOA composition and yield.

This study builds on the previous work on the *n*-dodecane low-NO_x system (Yee et al., 2012; Craven et al., 2012) employing complementary gas- (chemical ionization mass spectrometry) and particle-phase measurements (Aerodyne high-resolution time-of-flight aerosol mass spectrometry). We focus on the effect of alkane structure on the multi-generation gas-phase oxidation and particle-phase chemistry that leads to SOA formation. Of speical interest is the identification of and incorporation of multi-

Effect of chemical structure on SOA formation

L. D. Yee et al.

Title Page

Abstract | Introduction

Conclusions | References

Tables | Figures

◄ | ►

◄ | ►

Back | Close

Full Screen / Esc

Printer-friendly Version

Interactive Discussion

functional hydroperoxides in the aerosol via accretion reactions in the form of peroxy-hemiacetal (PHA) formation as well as the chemical evolution of the aerosol as it ages.

2 Experimental section

2.1 Chamber experiments

The experiments in this study were conducted using the experimental protocols and controls as discussed in Yee et al. (2012) and Craven et al. (2012). The experiments and conditions are given in Table 2. The *n*-dodecane experiments are the same as those presented in Yee et al. (2012) and Craven et al. (2012), and are used here for additional analyses and comparisons to the other C_{12} structures.

Experiments were conducted in the dual $28\,m^3$ Caltech Environmental Chambers (Cocker et al., 2001; Keywood et al., 2004). The chambers were flushed for at least 24 h with dry purified air between experiments, resulting in particle number and volume concentrations $< 100\,cm^{-3}$ and $< 0.1\,\mu m^3\,cm^{-3}$, respectively. Particle number concentration and size distributions were measured using a coupled differential mobility analyzer (DMA, TSI model 3081) and condensation particle counter (TSI Model 3010). Hydroxyl radicals were generated by photolysis of H_2O_2. Experiments began with slow injection of $280\,\mu L$ of a 50% aqueous H_2O_2 solution in a glass trap submerged in a warm water bath at 35–$38\,°C$, via a $5\,L\,min^{-1}$ flow of pure air. The chamber was then seeded with atomized $0.015\,M$ aqueous ammonium sulfate solution to achieve a target initial seed volume of ~ 10–$15\,\mu m\,cm^{-3}$. Subsequently, the hydrocarbon was injected by delivering the appropriate liquid volume or solid mass amount for the desired chamber concentration into a glass bulb, gently heating the glass bulb, and flowing $5\,L\,min^{-1}$ of pure air over the hydrocarbon until evaporation was complete.

Temperature (T), relative humidity (RH), and concentrations of O_3, NO, and NO_x were continuously monitored. Experiments were run at temperatures ranging from 23–$26\,°C$ after an initial rise from $20\,°C$ upon irradiation. RH remained below 10% for all

experiments except for the cyclododecane 36 h experiment in which RH rose to about 20 % in the last six hours. NO levels remained below the 5 ppb$_v$ lower detection limit of the analyzer (Horiba, APNA 360) and measured NO$_2$ levels remained below 7 ppb$_v$ after irradiation began.

2.2 Gas- and particle-phase measurements

Hydrocarbon concentration was continuously monitored by Gas Chromatograph-Flame Ionization Detection (GC-FID) by taking 1.3 L samples of chamber air on Tenax adsorbent. The cartridge was loaded into the GC-FID (Agilent 6890N), desorbed, and injected onto an HP-5 column (15 m × 0.53 mm ID × 1.5 µm thickness, Hewlett-Packard). Gas-phase oxidation products were monitored using a Chemical Ionization Mass Spectrometer (CIMS), consisting of a custom-modified Varian 1200 triple quadrupole mass spectrometer (Crounse et al., 2006; Paulot et al., 2009; St. Clair et al., 2010). Briefly, the instrument was operated in negative mode with CF$_3$OOCF$_3$ reagent gas, generating cluster products from the analyte at [X·CF$_3$O]$^-$ and F transfer products at [X·F]$^-$. The cluster product tends to occur when the analyte, X, is a hydroperoxide or weakly acidic compound. The transfer product dominates for more strongly acidic compounds. Several carboxylic acids are present in both ionizations, and are therefore reported as the sum of the two products when used. The negative mode mass scan ranged from *m/z* 50–300. Positive mode ionization utilizes water as the reagent gas and results in ion clusters of the form [X·(H$_2$O)$_n$H]$^+$. The positive mode mass scan ranged from *m/z* 50–200.

Due to mid-project tuning shifts in the positive mode operation, the ions monitored were not those expected from the ionization of proposed products. The reported ions are those as monitored during the project, though the proposed ion assignments are reported taking the tuning shift into account. A back-calibration was performed to verify the shift in peak-centering, which typically resulted in an upwards shift by 5 amu in the range of 200–220 amu during positive mode operation. To distinguish between ions

Title Page

Abstract | Introduction

Conclusions | References

Tables | Figures

|◄ | ►|

◄ | ►

Back | Close

Full Screen / Esc

Printer-friendly Version

Interactive Discussion

monitored in the different modes of the instrument a (+) or (−) is indicated in front of the *m/z* monitored for ions monitored in positive and negative mode operation, respectively.

An Aerodyne high-resolution time-of-flight aerosol mass spectrometer (DeCarlo et al., 2006), hereafter referred to as the AMS, was operated at 1 min resolution switching between the lower resolution, higher sensitivity "V-mode", and the high-resolution "W-mode". Data analysis and calibrations were performed according to procedures previously described (Allan et al., 2004; Aiken et al., 2007, 2008; Canagaratna et al., 2007). HR-ToF-AMS data were processed with Squirrel, the ToF-AMS Unit Resolution Analysis Toolkit and PIKA (Peak Integration by Key Analysis, DeCarlo et al., 2006), the high-resolution analysis software tool (http://cires.colorado.edu/jimenez-group/ToFAMSResources/ToFSoftware/index.html), in Igor Pro Version 6.22A (Wavemetrics, Lake Oswego, OR). At the beginning of each experiment, an AMS sample was taken with a particle filter in-line to the chamber sample line to make corrections for air interferences (Allan et al., 2004). The adjustments to the fragmentation table proposed by Aiken et al. (2008) for organic mass at *m/z* 18 and *m/z* 28 were included. Elemental ratios were calculated using the technique outlined by Aiken et al. (2007, 2008). The $C_2H_4^+$ ion at *m/z* 28 was not fit in PIKA due to strong interference from N_2^+, and was therefore not included in the elemental ratio calculations.

Photochemical simulations of each system were performed based on that of *n*-dodecane used in Yee et al. (2012) to further define the level of NO. An initial NO level of $\leq 1\,ppb_v$ is consistent with $\leq 10\,\%$ of reactions of RO_2 being due to reaction with NO_x. This NO concentration is also consistent with the trends observed for NO_x-sensitive species such as the first generation hydroperoxide and the 1,4-hydroxycarbonyl. Multifunctional nitrate species in the CIMS spectra were not significant, supporting that the $RO_2 + NO_x$ channels are not significant in these experiments.

Effect of chemical structure on SOA formation

L. D. Yee et al.

Title Page

Abstract | Introduction

Conclusions | References

Tables | Figures

|◄ | ►|

◄ | ►

Back | Close

Full Screen / Esc

Printer-friendly Version

Interactive Discussion

3 SOA formation chemistry

3.1 Chemical mechanism leading to SOA formation

A generalized mechanism for the photooxidation of alkanes under low-NO_x conditions (i.e. RO_2 reacts exclusively with HO_2) is presented in Fig. 1. This scheme is based on the *n*-dodecane photooxidation mechanism developed in Yee et al. (2012) generalized to the C_{12} structures studied here. R_1 and R_2 represent alkyl groups. In the case of *n*-dodecane, R_1 and R_2 are any straight-chain alkyl groups that sum to C_7H_{16}. For 2-methylundecane, R_1 and R_2 are also alkyl groups that make up C_7H_{16}, though one side contains a methyl branch at the number 2 carbon atom. For hexylcyclohexane, R_1 is C_6H_5 and R_2 is CH_3. While the sites of oxidation are shown in the mechanism to occur between R_1 and R_2, oxidation can also occur on the R_1 and R_2 groups including the C_6H_5 ring in hexylcyclohexane. In the case of cyclododecane, R_1 and R_2 are bonded together, indicated as R in the sidebar denoted by an asterisk. Structures in a solid box indicate one isomer of a product identified by the CIMS in the gas phase or the AMS in the particle phase. Colors of boxes containing compounds are consistent with those used when comparing trends of species in later plots within a compound system. Product names within the boxes will continue to be referenced in the following discussion, tables of identified products, and figures.

Photooxidation begins with H-abstraction by OH from the parent alkane (RH) to form an alkylperoxy radical (RO_2). Under the experimental conditions, the fate of the RO_2 radical is dominated by reaction with HO_2 radical ($\geq 90\%$), to form the 1st-generation hydroperoxide (ROOH). The hydroperoxide (ROOH) can then undergo reaction with OH (Channels 1 and 2) or photolysis (Channel 3). Along Channel 1, a 2nd-generation carbonyl (CARB) is formed, followed by continued oxidation to form a 3rd-generation carbonyl hydroperoxide (CARBROOH). This CARBROOH can also be generated via Channel 2, in which ROOH undergoes reaction with OH to generate a dihydroperoxide (DIROOH). In the case of Channel 1 where the carbonyl hydroperoxide forms such that the functional groups are on adjacent carbons (α-CARBROOH), photolysis of the

hydroperoxy group (Channel 1a) results in formation of an aldehyde (ALD) and several $< C_{12}$ fragments: peracid (C_nPACID), carboxylic acid (C_nCARBACID), and hydroperoxides (C_nROOH).

Along Channel 2, the carbonyl hydroperoxide (CARBROOH) can undergo photolysis (Channel 2a) analogous to the reactions outlined in Channel 3, or react with OH (Channel 2b). Channels 2a and 2b both lead to higher functionalized products. There is potential for tri-functionalized compounds (not shown) to form, a hydroxy carbonyl hydroperoxide (OHCARBROOH) to be formed along Channel 2a and a dicarbonyl hydroperoxide (DICARBROOH) along Channel 2b. Additional oxidation (not shown) can lead to a tricarbonyl hydroperoxide (TRICARBROOH) and hydroxy dicarbonyl hydroperoxide (OHDICARBROOH). The carbonyl hydroperoxide (CARBROOH), has a pure liquid vapor pressure ranging from 6.1×10^{-9} to 6.6×10^{-8} atm depending on structure, as estimated using the EVAPORATION method (Compernolle et al., 2011). This intermediate volatility/semi-volatile organic is one of the first products that can partition to the particle phase, Channel 2c.

In Channel 3, photolysis of the 1st-generation hydroperoxide produces an alkoxy radical RO. The C_{12} alkoxy radical will undergo 1,4-isomerization according to well-established mechanisms (Atkinson, 1997; Lim and Ziemann, 2005, 2009a,b). This results in the formation of a 1,4-hydroxy hydroperoxide (OHROOH) which has sufficiently low volatility to partition into the particle-phase or undergo reaction with OH or photolyze to generate a 1,4-hydroxy carbonyl (OHCARB). The 1,4-hydroxy carbonyl is known to undergo cyclization under an acid-catalyzed process on the particle surface to generate a cyclic hemiacetal (CHA) and dehydrate to form a dihydrofuran (DHF), which can then return to the gas phase to become further oxidized (Aschmann et al., 2003; Lim and Ziemann, 2009c).

In the case of cyclododecane where the ring strain is high enough (Benson, 1976; Lim and Ziemann, 2009a), the alkoxy radical can decompose to generate an aldehydic alkyl radical and a hydroperoxy aldehyde according to the starred scheme to the side (Fig. 1). Though a C_6 ring is not considered to have ring strain (Benson, 1976; Lim

Title Page

Abstract | Introduction

Conclusions | References

Tables | Figures

◄ | ►

◄ | ►

Back | Close

Full Screen / Esc

Printer-friendly Version

Interactive Discussion

and Ziemann, 2009a), hexylcyclohexane may also undergo ring opening in an analogous process depending on the extent and position of functionalization on the ring and its alkyl chain during continued oxidation. By structure activity estimations (Kwok and Atkinson, 1995), initial H-absraction by OH should primarily take place at the secondary carbons over the branching point in an approximate 80 % to 20 % ratio. Continued oxidation will tend to favor these secondary carbon sites over the branching point, though eventually fragmentation may be induced.

Several multi-functional hydroperoxides can potentially react with the aldehydes generated in Channel 1a to form peroxyhemiacetals. The carbonyl hydroperoxide PHA (CARBROOHPHA) is explicitly shown in the mechanisms (Figs. 1 and 2, Scheme 1), and was proposed as a key component of the initial SOA growth in the case of *n*-dodecane (Yee et al., 2012). Multi-functional PHAs are represented generally in Fig. 1, where Y is any functional group (-hydroxyl, -carbonyl, -hydroperoxy). The more explicit representation of expected higher functionalized products along Channel 2, and their potential to form PHAs is represented along the right-hand side of Fig. 2. One isomer is shown with the expected functionalization. PHA formation from DIROOH (Fig. 1, Channel 2) and OHROOH (Fig. 1, Channel 3) is not explicitly shown since these tracer ions are relatively small signals compared to those of other multi-functional hydroperoxides in the AMS. Of note is the potential to generate a 2nd-generation C_{12} hydroperoxy aldehyde in the case of cyclododecane, which is a likely candidate for participating in peroxyhemiacetal formation. Under Channels 1 and 2, the CARBROOH is a 3rd-generation product, though continued reaction with OH in these channels may compete with one generation of OH reaction and photolysis to form the hydroperoxy aldehyde.

3.2 Gas- and particle-phase product identification using CIMS and AMS

Ions monitored by the CIMS and the AMS and their proposed compound assignments by system are presented in Tables 3–7. Note that because hexylcyclohexane and cyclododecane differ by one degree of unsaturation from that of 2-methylundecane and

n-dodecane, many of the ions monitored across sytems for analogous products differ by just 2 amu.

3.2.1 Gas-phase mechanism comparison

Assuming that the CIMS sensitivity to certain functionalized species within the same mode of operation are comparable despite difference in structure (straight, branched, cyclic + branched, cyclic), comparisons of the several analogous gas-phase species help elucidate the chemical development by structure. These CIMS signals are normalized by the total reacted hydrocarbon to account for differences in initial hydrocarbon loading and represented along an OH exposure time scale for comparison of the different systems (Fig. 3). While there are slight differences in magnitude of the curves presented, gas-phase yields are not inferred from these figures as slight variations in the CIMS sensitivity based on structure may account for this effect.

The OH exposure in the system is defined as the product of the concentration of OH (molec cm^{-3}) and the hours of irradiation. The OH concentration is inferred from the initial hydrocarbon decay using the known reaction rate coefficient with OH. The OH concentration over the course of an experiment is constant ($\sim 2 \times 10^6$ molec cm^{-3}). Total OH exposure ranges from $\sim 8 \times 10^7$ molec cm^{-3} h to $\sim 1 \times 10^8$ molec cm^{-3} h for these experiments.

The 1st-generation hydroperoxides (ROOH) trends across systems are shown in Fig. 3, top panel. Under similar OH exposures the hexylcyclohexane hydroperoxide peaks slightly earlier than those of *n*-dodecane and cyclododecane. This is consistent with a slightly faster reaction rate coefficient for hexylcyclohexane. The 2nd-generation carbonyl (CARB) formation is compared across the systems in Fig. 3, middle panel. The trends are consistent with faster gas-phase oxidation for hexylcyclohexane.

Most of the intermediate hydroperoxide species are best monitored in negative mode operation of the CIMS, but due to the mass scan range ending at 300 amu, alternative ions in positive mode were used to track development of some expected products. Major products such as the carbonyl hydroperoxide (CARBROOH) for the 2-

methylundecane and *n*-dodecane systems were monitored at (+) *m/z* 204 for this reason (Table 3), while for hexylcyclohexane and cyclododecane CARBROOH was monitored at (−) *m/z* 299 (Table 4). Note that signal intensities should not be compared across positive and negative mode operation of the CIMS, as the sensitivities differ. The CARBROOH trends in Fig. 3 (bottom panel) show similar trends, though the signals are more noisy as this hydroperoxide is expected to be the first species with sufficiently low volatility to partition into the particle phase.

Many of the semi-volatile, higher functionalized products (OHROOH, OHCARBROOH, and DICARBROOH) while observed in Yee et al. (2012), were of too low signal to report for hexylcyclohexane and cyclododecane. A small signal with a trend consistent with the expected kinetics for the DICARBROOH in the 2-methylundecane system exists, indicating that this system does achieve this extent of oxidation in the gas-phase. However, the lack of expected signals in the gas-phase for all systems besides *n*-dodecane is likely a result of several factors. First, these multi-functional species are of sufficiently low vapor pressure to partition into the particle phase. Second, the experimental design utilized lower initial hydrocarbon loadings (to achieve comparable organic growth) moving towards the more cyclic structure of the studied compounds, lowering the overall production of such species in the gas-phase compared to their more straight-chain analogs. Finally, compounds like 2-methylundecane and hexylcylohexane may undergo more fragmentation processes leading to scission of the C_{12} chain and thereby less C_{12} multi-functional products owing to the potential to form tertiary alkoxy radicals.

3.2.2 Particle-phase composition

Mass spectra (1–2 h averages) from the AMS at the time of initial growth, a period mid-experiment, and at experiment end for each system, along with a difference spectrum from end and initial growth, are presented in Figs. 4–7. The initial growth spectrum is taken at the point where the organic mass rises above the limit of detection. The limit of detection is defined as 3 standard deviations above the signal during the filter period

taken before photooxidation begins. The mid-experiment average spectrum is taken at the point where the suspended organic is the highest, typically coincident with the peak of one or more AMS ion tracers of interest. The peak in suspended organic is consistent with the effects of particle wall loss and unlikely due to evaporation as the size distribution remains the same. The end spectrum is the average of the spectra during the last 1–2 h of photooxidation. The $C_xH_yO_z$ chemical formulas corresponding with the dominant exact masses are labeled in the mass spectra. Unit mass m/z is denoted here for brevity, but the reported ion chemical formulas are determined from the exact mass ions.

A few observations of the spectra are noted here. The mass spectrum from the hexylcyclohexane system (Figs. 6) between m/z 100–200 amu is less discretely structured as compared to the other compounds (Figs. 4, 5, 7). Since hexylcyclohexane exhibits alkyl, cyclic, and branched features in its structure, this may be realized as a unique "chaos" from this hybrid of chemical features in the aerosol spectrum. Overall, the difference spectra in the m/z 100–300 amu region are all positive, indicating the incorporation of higher molecular weight species. The only negative differences in signal are in the $m/z < 100$ range and are the result of alkyl ion fragments decreasing in the particle phase. Several ions in the >150 amu range have been proposed as tracers for particle-phase chemistry, as, though low in signal, they retain more molecular information. The chemical processes by which these >150 amu ions are generated may be analogous across all systems, as the structure of the spectra in this range are generally the same. That is, the prominent ions in hexylcyclohexane correspond to the prominent ions in the n-dodecane and 2-methylundecane cases, but tend to have one additional degree of unsaturation. This is consistent with the difference in degrees of unsaturation between the parent compounds. However, the cyclododecane peaks in this high amu region tend to be two degrees of unsaturation lower than those of n-dodecane. This could indicate chemical processing that results in more carbonyl group formation for the case of cyclododecane. This type of functionalization is relevant for cyclododecane along Channel 3 in the gas-phase mechanism (Fig. 1), as cyclododecane can

Effect of chemical structure on SOA formation

L. D. Yee et al.

Title Page

Abstract | Introduction

Conclusions | References

Tables | Figures

|◄ | ►|

◄ | ►

Back | Close

Full Screen / Esc

Printer-friendly Version

Interactive Discussion

ring-open early on, generating an aldehyde. This also means that cyclododecane can form a lower vapor pressure C_{12} aldehyde that can participate in particle-phase reactions as discussed in Lim and Ziemann (2009a,b), whereas other systems form a $<C_{12}$ aldehyde along Channel 1a (Fig. 1).

3.2.3 Indicators of particle-phase chemistry: peroxyhemiacetal (PHA) formation

Yee et al. (2012) and Craven et al. (2012) proposed that several ion tracers in the $m/z >150$ amu region differing by 32 amu could be used to track a variety of potential peroxyhemiacetals (PHAs) formed in the particle-phase. Craven et al. (2012) established that general hydroperoxides (ROOH) could be monitored in the AMS at ions consistent with an m/z [M-33]$^+$, where M is the molecuar weight of the hydroperoxide. This ion will be hereafter referred to as R$^+$. However, the distinct pattern of similarly trending ions >150 amu that are 32 amu apart suggests that this mass difference may result from the peroxide O−O bond of a peroxyhemiacetal. We refer to this ion as ROO$^+$ for the following discussions. These ions are listed in tables of ions monitored in the AMS along with their proposed product assignments (Tables 5–7). Since these initial studies, another n-dodecane experiment (not presented here) involved intentional injection of tridecanal in the dark after an initial period of dodecane photooxidation and SOA formation to induce peroxyhemiacetal formation. Upon tridecanal injection, a corresponding decrease in signal of several hyderoperoxide species occurred in the gas-phase (as monitored by the CIMS) accompanied by a corresponding increase in the 32 amu difference ion pairs in the AMS, consistent with the proposed attribution to particle-phase chemistry involving peroxyhemiacetal formation.

The formation of fragments along Channel 1a, specifically carboxylic acids tracked by the CIMS, is the key proxy for the presence of aldehyde in the system (since the aldehyde is not directly measured). The presence of gas-phase acid indicates that peroxyhemiacetal formation may commence, as observed in Yee et al. (2012) for n-dodecane. Hence, a key comparison of the gas and particle-phase measurements includes the time trend comparison between gas-phase acid production and particle-

phase ion markers for PHA formation. In each system, the CARBROOH PHA ions grow in the particle phase when gas-phase acid forms, as indicated by the C_6 carboxylic acid, C6CARBACID, in Fig. 8. The initial growth of organic in each of these systems is also characterized by the respective CARBROOH and CARBROOH PHA tracer ions in the AMS mass spectra. In Figs. 4 and 5, $C_{12}H_{23}O^+$ at *m/z* 183 and $C_{12}H_{23}O_3^+$ at *m/z* 215 are the dominant ions at initial growth of *n*-dodecane and 2-methylundecane SOA. For hexylcyclohexane (Fig. 6) and cyclododecane (Fig. 7), the ion at $C_{12}H_{21}O_3^+$ at *m/z* 213 is characteristic of initial growth. Note that there are different right hand axes and scales for the R^+ and ROO^+ ion tracers in Fig. 8.

3.2.4 Effect of structure on PHA formation

The general particle-phase development is shown in terms of the multi-functional hydroperoxide/PHA R^+ and PHA ROO^+ proposed ion tracers for all systems (Fig. 9). All ion signals have been normalized by the suspended organic to account for effects on the ion signal trend due to particle wall loss. This normalization results in large noise at periods < OH exposure of 2×10^7 molec cm^{-3} h, owing to low and noisy ion and organic signals before this time. The same tracer ions are present in both the *n*-dodecane and 2-methylundecane systems (Fig. 9a and b). $C_{12}H_{19}O_5^+$ is of low signal in the 2-methylundecane and *n*-dodecane AMS spectra, though there is a greater contribution from this ion in *n*-dodecane SOA. All of these ions can potentially be explained by multi-functional hydroperoxide compounds that can carry up to four sites of functionalization and three degrees of unsaturation relative to the parent (See PHA schemes in Fig. 2 for proposed multi-functional structures and AMS ions assignments in Table 5). Generally, the CARBROOH is initially incorporated, followed by the DICARBROOH ($C_{12}H_{21}O_2^+$ at *m/z* 197) and the OHCARBROOH ($C_{12}H_{23}O_2^+$ at *m/z* 199). Additional chemical processing leads to incorporation of a potential OHDICARBROOH ($C_{12}H_{21}O_3^+$ at *m/z* 213) and a TRICARBROOH ($C_{12}H_{19}O_3^+$ at *m/z* 211). The $C_{12}H_{19}O_5^+$ at *m/z* 245 is possibly the OHDICARBROOH PHA ROO^+ ion, though the signal at this *m/z* is not sufficiently high to be plotted on the same scale as the R^+ ions here. The DIROOH and OHROOH

tracer ions are also not included for this reason, although tracer ions are identified in the mass spectra. Of note is the relatively earlier peaking (in terms of OH exposure) and lower relative contribution of these ions in the 2-methylundecane system as compared to their analogs in the *n*-dodecane system. This may be a result of fragmentation processes relevant for 2-methylundecane gas-phase oxidation that begin to dominate. The lower relative contribution of $C_{12}H_{19}O_5^+$ for 2-methylundecane SOA as compared to *n*-dodecane SOA is also consistent with less chemical development due to gas-phase fragmentation dominating over functionalization, as well as potentially slower gas-phase oxidation since 2-methylundecane has a lower k_{OH} than that of *n*-dodecane.

For hexylcyclohexane, there is noticeably more simultaneous incorporation in the aerosol phase of such species as the CARBROOH ($C_{12}H_{21}O^+$ at *m/z* 181), DICARBROOH ($C_{12}H_{19}O_2^+$ at *m/z* 195), OHCARBROOH ($C_{12}H_{21}O_2^+$ at *m/z* 197), and their respective PHAs (Fig. 9c, Table 6). There is also significant contribution from an ion at $C_{12}H_{19}O^+$, not explained by the PHA tracer fragmentation pattern. The presence of the $C_{12}H_{19}O^+$ ion may be a result of forming an analogous hydroperoxy dihydrofuran product (Fig. 2, Scheme 3) via the OHCARBROOH undergoing 1,4 cyclization and dehydration. This ion is unique to hexylcyclohexane SOA (in terms of degrees of unsaturation achieved with little oxygen in the ion formula and prominence of the ion). The proposed reaction is consistent with the hexylcyclohexane structure affording another 1,4-cyclization due to its C_6 branch. This also forms a dihydrofuran-like structure of higher volatility. This prominent route may therefore limit formation of lower volatility oxidation products during hexylcyclohexane oxidation. The peak of the suspended organic (Fig. 9c, OH exposure $\sim 5 \times 10^6$ molec cm^{-3} h) does follow the peak of this ion and those of the DICARBROOH, OHCARBROOH, consistent with limitations of the growth. At this point the rate of particle wall loss dominates over the rate of continued growth.

Tracer ions for these products are followed by further chemical processing leading also to the OHDICARBROOH and its PHA ($C_{12}H_{19}O_3^+$ at *m/z* 211) and the OHDICAR-

Title Page

Abstract | Introduction

Conclusions | References

Tables | Figures

|◄ | ►|

◄ | ►

Back | Close

Full Screen / Esc

Printer-friendly Version

Interactive Discussion

BROOH PHA ($C_{12}H_{19}O_5^+$ at m/z 243). The m/z 243 ion is not shown due to low signal. The ion at m/z 227 $C_{12}H_{19}O_4^+$ corresponds to the ROO^+ ion for DICARBROOH PHA, though the time trend does not follow that of the R^+ ion as closely, and may indicate another species (in combination) being responsible for the signal here. For example, in Fig. 2, Scheme 5, the OHDICARBROOH may isomerize (left reaction) via cyclization between a carbonyl and hydroperoxy group to form this ion as well. It may also undergo 1,4-cyclization involving the hydroxy and ketone groups. This presents two potentially competitive fates for the OHDICARBROOH, one to PHA formation (Scheme 5, right reaction) and cyclization (Scheme 5, left and bottom reaction). Cyclization of alkoxy hydroperoxy aldehydes has been observed to be potentially competitive with PHA formation in the case of cyclic alkenes ozonolysis in the presence of alcohols (Ziemann, 2003). A similar cyclization reaction for the multi-functional carbonyl hydroperoxides can explain the presence of additional ions not expected from PHA formation.

For cyclododecane, at least two "waves" of chemical development exist in the particle phase (Fig. 9d). Initially, R^+ ions associated with the CARBROOH, OHCARBROOH, and DICARBROOH grow in. Then, a series of ions with formulae of the form $C_{12}H_yO_3^+$, with $y = 19$, 17, and 15 grow in consecutively. $C_{12}H_{19}O_3^+$ at m/z 211 and $C_{12}H_{17}O_3^+$ at m/z 209 could correspond with the OHDICARBROOH and TRICARBROOH R^+ ions, respectively. Note that the $C_{12}H_{19}O_3^+$ ion can also result from a ring-opened TRICARBROOH (same as in the linear case), but where at least one of the carbonyl groups is presumably an aldehyde. The $C_{12}H_{15}O_3^+$ at m/z 207 implies yet another step achieving one fewer degree of saturation. This was characteristic of many of the ions in the cyclododecane AMS mass spectra achieving one additional degree of unsaturation compared to that of hexylcyclohexane and two compared to the non-cyclic systems. This ion assignment is uncertain, though it could correspond with a structure containing a hydroxy, four ketone groups, and a hydroperoxy group with the ring intact (OH4CARBROOH). There may be additional cyclizations or dehydration reactions in the particle phase and/or additional ionzation patterns in the AMS that may more feasibly explain the presence of this ion. This is especially relevant when con-

sidering the ions of the form $C_{12}H_yO_z^+$, with $y = 19$, 17, and 15 and $z = 3$, 4, 5. For the OH4CARBROOH, TRICARBROOH, and OHDICARBROOH the mass spectrum (Fig. 7) indicates a greater fraction of organic due to the corresponding $z = 4$ ions compared to the $z = 5$ ions. This may indicate competitive cyclization over PHA formation as shown in Schemes 4 (TRICARBROOH) and 5 (OHDICARBROOH) of Fig. 2.

Common for all four systems, three ions that enter the particle phase early on (within 2×10^7 molec cm^{-3} h OH exposure) are attributed to their respective CARBROOH, OHCARBROOH, and DICARBROOH. While the R^+ ions can come from both the hydroperoxide itself and its derived PHA, the ROO$^+$ ion is considered to arise mostly from PHA. To understand the effect of structure on PHA formation, time trends of the fraction of the organic attributed to ROO$^+$ PHA tracer ions can be compared across parent structures. These analyses assume that the ionization probability and fragmentation pattern in the AMS are relatively consistent for PHAs of analogous functionaility. For example, the CARBROOH PHA ionization probability is similar across the four C_{12} alkanes studied. Also, this currently assumes that there is only one hydroperoxide and its PHA (regardless of the aldehyde variety) contributing to the ROO$^+$.

Figure 10 shows that the relative fraction of organic attributed to the CARBROOH PHA is approximately similar for *n*-dodecane and hexylcyclohexane, followed by 2-methylundecane and cyclododecane (top panel). For the DICARBROOH PHA (middle panel) and OHCARBROOH PHA (bottom panel), a greater fraction of the organic is attributed to PHAs in hexylcyclohexane SOA, followed by *n*-dodecane. Smaller contributions are made for the PHAs from 2-methylundecane and cyclododecane. Generally, the fraction of organic attributed to the cyclododecane-derived PHAs is lower compared to the other systems, indicating that there may be structural biases in PHA formation. Since PHA formation relies on the intermolecular reaction of two condensing species, aldehyde and a hydroperoxide, it may be that the cyclic structure of cyclododecane is less apt for this reaction. There is also trend information in Fig. 8d that shows that the R^+ and ROO$^+$ ions for CARBROOH PHA in cyclododecane do not trend together as tightly as compared to the other systems (Fig. 8a–c). The ROO$^+$ ion lags slightly,

Title Page

Abstract | Introduction

Conclusions | References

Tables | Figures

|◄ | ►|

◄ | ►

Back | Close

Full Screen / Esc

Printer-friendly Version

Interactive Discussion

indicating that PHA formation from the CARBROOH in cyclododecane may not form immediately with the condensation of CARBROOH.

While signal at the ROO$^+$ ion for CARBROOH PHA can also potentially be derived from the OHCARBROOH cyclizing as in Fig. 2, Scheme 3, the tight correlation of the R$^+$ and ROO$^+$ ions for *n*-dodecane and 2-methylundecane suggests less of a contribution from competing cyclization. Since the R$^+$ ions cannot be derived from the competitive cyclization products, the majority of the signal at the ROO$^+$ ion is attributed to the CARBROOH PHA form. For hexylcyclohexane and cyclododecane, however, there is slightly more deviation of the R$^+$ and ROO$^+$ ion trends. This may suggest that these structures may undergo intramolecular reactions that result in the variety of ions and chemical development as discussed earlier.

3.2.5 AMS elemental ratios

The Van Krevelen diagram, originally used for showing how O:C and H:C elemental ratios change during coal formation (Van Krevelen, 1950), has been recently utilized with HR-TOF-AMS data to aid in the interpretation of elemental ratio changes in organic aerosol formation (Heald et al., 2010; Ng et al., 2011; Chhabra et al., 2011; Lambe et al., 2011, 2012). The slopes on the diagram of O:C versus H:C can provide insight into the chemical evolution of the aerosol in terms of functional group changes. A slope of −1 for ambient and laboratory data is consistent with carboxylic acid groups without fragmentation (Heald et al., 2010). Ng et al. (2011), showed that for aged ambient organic aerosol, the slope of −0.5 is consistent with carboxylic acid addition with fragmentation. Both of these results highlighted aerosol that was already quite oxidized, with most of the O:C values greater than 0.30. Lambe et al. (2012) presented SOA results from a Potential Aerosol Mass (PAM) chamber in which long-chain alkane SOA O:C extended from a value of 0 to close to 1.4. The Van Krevelen slope from an O:C of 0 to approximately 0.3 was −1.3, and for O:C values greater than 0.3 the slope became less negative with a value of −0.7. Lambe et al. (2012) attribute this change in slope to a transition from a functionalized- to fragment-dominated regime.

The elemental ratios from the current study are shown in Fig. 11. The experimental progression for all four systems is from upper left to lower right across the Van Krevelen space. All of the compounds have O:C < 0.3, except for the end of the hexylcyclohexane experiment. In increasing order, the slopes are -1.73, -1.35, -1.19, and -1.14

5 for cyclododecane, 2-methylundecane, dodecane, and hexylcyclohexane. The higher O:C achieved for hexylcyclohexane may be a result of the generally faster chemistry seen in both the gas-phase oxidation and the particle-phase development, in which initial key ions in the particle phase (Fig. 9c) peak earlier in terms of OH exposure $< 5 \times 10^7$ molec cm^{-3} h as compared to those of the other systems. This could be a

10 result of fragmentation processes increasing the O:C or oxygenation achieved from continued oxidation.

n-Dodecane achieves the next highest O:C for the OH exposures in this study, and while the progression of key >150 amu ions in this system (Fig. 9a) is more gradual, there is continued oxygenation, as observed by the presence of the $C_{12}H_{19}O_5^+$ ion.

15 Yee et al. (2012) also found the O:C range to be consistent with the O:C of several of the multi-functional hydroperoxides and their derived PHAs. 2-methylundecane SOA exhibits a lower O:C than that from *n*-dodecane, supported by the lower fraction of total organic attributed to oxidized ions, compared to *n*-dodecane.

Finally, cyclododecane SOA has the slope closest to -2, indicating a greater contri-

20 bution from ketone and aldehyde groups. This is consistent with the $C_{12}H_yO_3^+$ ion series in Fig. 9d and the relatively higher degrees of unsaturation in the cyclododecane AMS mass spectrum (Fig. 7) as compared to the other systems.

4 Conclusions

We address here the mechanisms of formation of SOA in alkane sytems under low-NO$_x$

25 conditions. Special attention is given to the effect of alkane structure on SOA formation and to the molecular identifications of the oxidation products responsible for SOA growth. Aerosol formation from the photooxidation of *n*-dodecane, 2-methylundecane,

hexylcyclohexane, and cyclododecane under low-NO_x conditions, is initiated by the partitioning of a 2nd-generation product, the carbonyl hydroperoxide (CARBROOH), to the particle phase. It appears that this hydroperoxide is incorporated with simultaneous formation of a peroxyhemiacetal. Several other multi-functional hydroperoxides are proposed to explain characteristic ions in the AMS mass spectra for each system, suggesting that at least three additional degrees of unsaturation might be achieved for cyclododecane while functionalizing primarily via ketone/aldehyde addition. Evidence for additional particle-phase reactions including cyclization of multi-functional hydroperoxides exists. Intramolecular cyclization of multi-functional hydroperoxides can be competitive with the intermolecular reaction of multi-functional hydroperoxides with aldehydes to form PHAs.

2-methylundecane exhibits the least extent of chemical processing relative to the other systems, likely a result of gas-phase fragmentation that leads to a product distribution consisting of relatively higher volatility intermediates. Hexylcyclohexane exhibits rapid gas-phase oxidation and particle-phase processing reflected in the highest achieved O:C (verging on 0.4). Of the systems studied, hexylcyclohexane behaves in terms of SOA chemistry somewhere between 2-methylundecane and cyclododecane. It exhibits the rapid formation of functionalized semi- and low-volatility species that contribute to the particle phase, but then fragmentation processes (attributable to the branching) start to dominate and lower the relative particle mass due to C_{12} oxygenates. Cyclization processes analogous to cyclic hemiacetal and higher volatility dihydrofuran formation can also contribute to limitations in particle growth.

While the >150 amu tracer ions in the AMS help to identify potential species involved in particle-phase chemistry like PHA formation, the more oxidized and functionalized the ion, the greater potential exists for multiple ionization and fragmentation schemes in the AMS. Ideally, standards of different structure, but analogous functionality would be necessary to better understand the mass spectra in this region. Ionization schemes that include possibilities of cyclic and/or cyclization followed by dehydration of compounds in the particle phase are necessary. Such schemes were proposed here to explain

Title Page

Abstract | Introduction

Conclusions | References

Tables | Figures

◄ | ►|

◄ | ►

Back | Close

Full Screen / Esc

Printer-friendly Version

Interactive Discussion

additional ions in the AMS not expected purely from PHA formation. This is relevant for determining the molecular identity of some of the highly oxygenated ($>O_3^+$) ions that grow in the particle phase at extended OH exposures.

For the functional groups presumed to be incorporated via the gas-phase mechanism, ketone (some aldehyde for cyclododecane), hydroperoxy, and hydroxyl, it is very likely these functional groups undergo intramolecular, as well as intermolecular, reactions (including oligomer formation) depending on their relative positions on the C_{12} backbone. This may be highly relevant for hexylcyclohexane in which the alkyl branch is sufficiently long to still cyclize and result in a bicyclic structure. Cyclododecane may ring open to form functionalized aldehydes and then cyclize again (not necessarily returning to a C_{12} ring).

The systematic study of these C_{12} structures lays a chemical groundwork for understanding the dynamics of particle growth concerted with particle-phase reactions (e.g. PHA formation) and sustained growth via semi-volatile and low-volatile product partitioning, followed by additional particle-phase oxidation if unhampered by fragmentation processes. Further study of the C_{12} system should include additional isomeric configurations of branching and cyclic + branched structures to understand better the spectrum of oxidation pathways between 2-methlyundecane and hexylcyclohexane and between hexylcyclohexane and cyclododecane. These structural dependencies will certainly impact the mechanisms of SOA formation and SOA yields, which can affect the representation of SOA formation from alkanes.

Effect of chemical structure on SOA formation

L. D. Yee et al.

Title Page

Abstract	Introduction
Conclusions	References
Tables	Figures

|◄ | ►|

◄ | ►

Back | Close

Full Screen / Esc

Printer-friendly Version

Interactive Discussion

References

Aiken, A. C., DeCarlo, P. F., and Jimenez, J. L.: Elemental analysis of organic species with electron ionization high-resolution mass spectrometry, Anal. Chem., 79, 8350–8358, 2007. 10864

Aiken, A. C., Decarlo, P. F., Kroll, J. H., Worsnop, D. R., Huffman, J. A., Docherty, K. S., Ulbrich, I. M., Mohr, C., Kimmel, J. R., Sueper, D., Sun, Y., Zhang, Q., Trimborn, A., Northway, M., Ziemann, P. J., Canagaratna, M. R., Onasch, T. B., Alfarra, M. R., Prevot, A. S. H., Dommen, J., Duplissy, J., Metzger, A., Baltensperger, U., and Jimenez, J. L.: O/C and OM/OC ratios of primary, secondary, and ambient organic aerosols with high-resolution time-of-flight aerosol mass spectrometry, Environ. Sci. Technol., 42, 4478–4485, 2008. 10864

Allan, J. D., Delia, A. E., Coe, H., Bower, K. N., Alfarra, M. R., Jimenez, J. L., Middlebrook, A. M., Drewnick, F., Onasch, T. B., Canagaratna, M. R., Jayne, J. T., and Worsnop, D. R.: A generalised method for the extraction of chemically resolved mass spectra from aerodyne aerosol mass spectrometer data, J. Aerosol Sci., 35, 909–922, 2004. 10864

Aschmann, S. M., Arey, J., and Atkinson, R.: Kinetics and products of the gas-phase reaction of OH radicals with 5-hydroxy-2-pentanone at 296±2 k, J. Atmos. Chem., 45, 289–299, doi:10.1023/A:1024216900051, 2003. 10861, 10866

Atkinson, R.: Gas-phas tropospheric chemistry of organic compounds, J. Phys. Chem. Ref. Data, Monogr., 2, 1–216, 1994. 10861

Atkinson, R.: Gas-phase tropospheric chemistry of volatile organic compounds. 1. Alkanes and alkenes, J. Phys. Chem. Ref. Data, 26, 215–290, 1997. 10861, 10866

Atkinson, R. and Arey, J.: Atmospheric degradation of volatile organic compounds, Chem. Rev., 103, 4605–4638, doi:10.1021/cr0206420, 2003. 10861

Atkinson, R., Arey, J., and Aschmann, S. M.: Atmospheric chemistry of alkanes: Review and recent developments, Atmos. Environ., 42, 5859–5871, doi:10.1016/j.atmosenv.2007.08.040, 2008. 10861

Aumont, B., Valorso, R., Mouchel-Vallon, C., Camredon, M., Lee-Taylor, J., and Madronich, S.: Modeling SOA formation from the oxidation of intermediate volatility n-alkanes, Atmos. Chem. Phys., 12, 7577–7589, doi:10.5194/acp-12-7577-2012, 2012. 10861

Bahreini, R., Middlebrook, A. M., de Gouw, J. A., Warneke, C., Trainer, M., Brock, C. A., Stark, H., Brown, S. S., Dube, W. P., Gilman, J. B., Hall, K., Holloway, J. S., Kuster, W. C., Perring, A. E., Prevot, A. S. H., Schwarz, J. P., Spackman, J. R., Szidat, S., Wag-

ner, N. L., Weber, R. J., Zotter, P., and Parrish, D. D.: Gasoline emissions dominate over diesel in formation of secondary organic aerosol mass, Geophys. Res. Lett., 39, L06805, doi:10.1029/2011GL050718, 2012. 10860

Benson, S. W.: Thermochemical kinetics, Wiley, second edn., 320 pp., 1976. 10866

5 Canagaratna, M., Jayne, J., Jimenez, J., Allan, J., Alfarra, M., Zhang, Q., Onasch, T., Drewnick, F., Coe, H., Middlebrook, A., Delia, A., Williams, L., Trimborn, A., Northway, M., DeCarlo, P., Kolb, C., Davidovits, P., and Worsnop, D.: Chemical and microphysical characterization of ambient aerosols with the Aerodyne aerosol mass spectrometer, Mass Spectrom. Rev., 26, 185–222, doi:10.1002/mas.20115, 2007. 10864

10 Cappa, C. D., Zhang, X., Loza, C. L., Craven, J. S., Yee, L. D., and Seinfeld, J. H.: Application of the statistical oxidation model (SOM) to secondary organic aerosol formation from photooxidation of C_{12} alkanes, Atmos. Chem. Phys., 13, 1591–1606, doi:10.5194/acp-13-1591-2013, 2013. 10861

Chhabra, P. S., Ng, N. L., Canagaratna, M. R., Corrigan, A. L., Russell, L. M., Worsnop, D. R.,
15 Flagan, R. C., and Seinfeld, J. H.: Elemental composition and oxidation of chamber organic aerosol, Atmos. Chem. Phys., 11, 8827–8845, doi:10.5194/acp-11-8827-2011, 2011. 10876

Cocker, D. R., Flagan, R. C., and Seinfeld, J. H.: State-of-the-art chamber facility for studying atmospheric aerosol chemistry, Environ. Sci. Technol., 35, 2594–2601, 2001. 10862

Compernolle, S., Ceulemans, K., and Müller, J.-F.: EVAPORATION: a new vapour pressure
20 estimation methodfor organic molecules including non-additivity and intramolecular interactions, Atmos. Chem. Phys., 11, 9431–9450, doi:10.5194/acp-11-9431-2011, 2011. 10866, 10886

Craven, J. S., Yee, L. D., Ng, N. L., Canagaratna, M. R., Loza, C. L., Schilling, K. A., Yatavelli, R. L. N., Thornton, J. A., Ziemann, P. J., Flagan, R. C., and Seinfeld, J. H.: Analysis of secondary
25 organic aerosol formation and aging using positive matrix factorization of high-resolution aerosol mass spectra: application to the dodecane low-NO$_x$ system, Atmos. Chem. Phys., 12, 11795–11817, doi:10.5194/acp-12-11795-2012, 2012. 10861, 10862, 10871

Crounse, J. D., McKinney, K. A., Kwan, A. J., and Wennberg, P. O.: Measurement of gas-phase hydroperoxides by chemical ionization mass spectrometry, Anal. Chem., 78, 6726–6732,
30 2006. 10863

DeCarlo, P. F., Kimmel, J. R., Trimborn, A., Northway, M. J., Jayne, J. T., Aiken, A. C., Gonin, M., Fuhrer, K., Horvath, T., Docherty, K. S., Worsnop, D. R., and Jimenez, J. L.:

Effect of chemical structure on SOA formation

L. D. Yee et al.

Title Page

Abstract | Introduction

Conclusions | References

Tables | Figures

|◄ | ►|

◄ | ►

Back | Close

Full Screen / Esc

Printer-friendly Version

Interactive Discussion

Field-deployable, high-resolution, time-of-flight aerosol mass spectrometer, Anal. Chem., 78, 8281–8289, 2006. 10864

Dibble, T. S.: Cyclization of 1,4-hydroxycarbonyls is not a homogenous gas phase process, Chem. Phys. Lett., 447, 5–9, doi:10.1016/j.cplett.2007.08.088, 2007. 10861

Gentner, D. R., Isaacman, G., Worton, D. R., Chan, A. W. H., Dallmann, T. R., Davis, L., Liu, S., Day, D. A., Russell, L. M., Wilson, K. R., Weber, R., Guha, A., Harley, R. A., and Goldstein, A. H.: Elucidating secondary organic aerosol from diesel and gasoline vehicles through detailed characterization of organic carbon emissions, Proc. Natl. Acad. Sci. USA, doi:10.1073/pnas.1212272109, 2012. 10860

Heald, C. L., Kroll, J. H., Jimenez, J. L., Docherty, K. S., DeCarlo, P. F., Aiken, A. C., Chen, Q., Martin, S. T., Farmer, D. K., and Artaxo, P.: A simplified description of the evolution of organic aerosol composition in the atmosphere, Geophys. Res. Lett., 37, L08803, doi:10.1029/2010GL042737, 2010. 10876

Isaacman, G., Wilson, K. R., Chan, A. W. H., Worton, D. R., Kimmel, J. R., Nah, T., Hohaus, T., Gonin, M., Kroll, J. H., Worsnop, D. R., and Goldstein, A. H.: Improved resolution of hydrocarbon structures and constitutional isomers in complex mixtures using gas chromatography-vacuum ultraviolet-mass spectrometry, Anal. Chem., 84, 2335–2342, doi:10.1021/ac2030464, 2012. 10860

Jenkin, M. E., Saunders, S. M., and Pilling, M. J.: The tropospheric degradation of volatile organic compounds: a protocol for mechanism development, Atmos. Environ., 31, 81–104, doi:10.1016/S1352-2310(96)00105-7, 1997. 10886

Jordan, C. E., Ziemann, P. J., Griffin, R. J., Lim, Y. B., Atkinson, R., and Arey, J.: Modeling SOA formation from OH reactions with C8-C17 n-alkanes, Atmos. Environ., 42, 8015–8026, doi:10.1016/j.atmosenv.2008.06.017, 2008. 10861

Keywood, M. D., Varutbangkul, V., Bahreini, R., Flagan, R. C., and Seinfeld, J. H.: Secondary organic aerosol formation from the ozonolysis of cycloalkenes and related compounds, Environ. Sci. Technol., 38, 4157–4164, 2004. 10862

Kwok, E. S. and Atkinson, R.: Estimation of hydroxyl radical reaction rate constants for gas-phase organic compounds using a structure-reactivity relationship: An update, Atmos. Environ., 29, 1685–1695, doi:10.1016/1352-2310(95)00069-B, 1995. 10867

Lambe, A. T., Onasch, T. B., Massoli, P., Croasdale, D. R., Wright, J. P., Ahern, A. T., Williams, L. R., Worsnop, D. R., Brune, W. H., and Davidovits, P.: Laboratory studies of the chemical composition and cloud condensation nuclei (CCN) activity of secondary organic aerosol

Title Page

Abstract | Introduction

Conclusions | References

Tables | Figures

|◄ | ►|

◄ | ►

Back | Close

Full Screen / Esc

Printer-friendly Version

Interactive Discussion

(SOA) and oxidized primary organic aerosol (OPOA), Atmos. Chem. Phys., 11, 8913–8928, doi:10.5194/acp-11-8913-2011, 2011. 10876

Lambe, A. T., Onasch, T. B., Croasdale, D. R., Wright, J. P., Martin, A. T., Franklin, J. P., Massoli, P., Kroll, J. H., Canagaratna, M. R., Brune, W. H., Worsnop, D. R., and Davidovits, P.: Transitions from functionalization to fragmentation reactions of laboratory secondary organic aerosol (SOA) generated from the OH oxidation of alkane precursors, Environ. Sci. Technol., 46, 5430–5437, doi:10.1021/es300274t, 2012. 10861, 10876

Lim, Y. B. and Ziemann, P. J.: Products and mechanism of secondary organic aerosol formation from reactions of n-alkanes with OH radicals in the presence of NO_x, Environ. Sci. Technol., 39, 9229–9236, doi:10.1021/es051447g, 2005. 10861, 10866

Lim, Y. B. and Ziemann, P. J.: Effects of molecular structure on aerosol yields from OH radical-initiated reactions of linear, branched, and cyclic alkanes in the presence of NO_x, Environ. Sci. Technol., 43, 2328–2334, doi:10.1021/es803389s, 2009a. 10861, 10866, 10871

Lim, Y. B. and Ziemann, P. J.: Chemistry of secondary organic aerosol formation from OH radical-initiated reactions of linear, branched, and cyclic alkanes in the presence of NO_x, Aerosol Sci. Technol., 43, 604–619, doi:10.1080/02786820902802567, 2009b. 10861, 10866, 10871

Lim, Y. B. and Ziemann, P. J.: Kinetics of the heterogeneous conversion of 1,4-hydroxycarbonyls to cyclic hemiacetals and dihydrofurans on organic aerosol particles, Phys. Chem. Chem. Phys., 11, 8029–8039, doi:10.1039/B904333K, 2009c. 10861, 10866

Lipsky, E. M. and Robinson, A. L.: Effects of dilution on fine particle mass and partitioning of semivolatile organics in diesel exhaust and wood smoke, Environ. Sci. Technol., 40, 155–162, 2006. 10861

Nakao, S., Shrivastava, M., Nguyen, A., Jung, H., and Cocker, D.: Interpretation of secondary organic aerosol formation from diesel exhaust photooxidation in an environmental chamber, Aerosol Sci. Technol., 45, 964–972, doi:10.1080/02786826.2011.573510, 2011. 10861

Ng, N. L., Canagaratna, M. R., Jimenez, J. L., Chhabra, P. S., Seinfeld, J. H., and Worsnop, D. R.: Changes in organic aerosol composition with aging inferred from aerosol mass spectra, Atmos. Chem. Phys., 11, 6465–6474, doi:10.5194/acp-11-6465-2011, 2011. 10876

Paulot, F., Crounse, J. D., Kjaergaard, H. G., Kroll, J. H., Seinfeld, J. H., and Wennberg, P. O.: Isoprene photooxidation: new insights into the production of acids and organic nitrates, Atmos. Chem. Phys., 9, 1479–1501, 1680-7316, 2009. 10863

Title Page

Abstract | Introduction

Conclusions | References

Tables | Figures

|◄ | ►|

◄ | ►

Back | Close

Full Screen / Esc

Printer-friendly Version

Interactive Discussion

Presto, A. A., Miracolo, M. A., Kroll, J. H., Worsnop, D. R., Robinson, A. L., and Donahue, N. M.: Intermediate-volatility organic compounds: a potential source of ambient oxidized organic aerosol, Environ. Sci. Technol., 43, 4744–4749, doi:10.1021/es803219q, 2009. 10861

Presto, A. A., Miracolo, M. A., Donahue, N. M., and Robinson, A. L.: Secondary organic aerosol formation from high-NO$_x$ photo-oxidation of low volatility precursors: n-alkanes, Environ. Sci. Technol., 44, 2029–2034, doi:10.1021/es903712r, 2010. 10861

Pye, H. O. T. and Pouliot, G. A.: Modeling the role of alkanes, polycyclic aromatic hydrocarbons, and their oligomers in secondary organic aerosol formation, Environ. Sci. Technol., 46, 6041–6047, doi:10.1021/es300409w, 2012. 10861

Robinson, A. L., Donahue, N. M., Shrivastava, M. K., Weitkamp, E. A., Sage, A. M., Grieshop, A. P., Lane, T. E., Pierce, J. R., and Pandis, S. N.: Rethinking organic aerosols: Semivolatile emissions and photochemical aging, Science, 315, 1259–1262, 2007. 10860

Schauer, J. J., Kleeman, M. J., Cass, G. R., and Simoneit, B. R. T.: Measurement of emissions from air pollution sources. 2. C1 through C30 organic compounds from medium duty diesel trucks, Environ. Sci. Technol., 33, 1578–1587, doi:10.1021/es980081n, 1999. 10860

Schauer, J. J., Kleeman, M. J., Cass, G. R., and Simoneit, B. R. T.: Measurement of emissions from air pollution sources. 5. C1-C32 organic compounds from gasoline-powered motor vehicles, Environ. Sci. Technol., 36, 1169–1180, doi:10.1021/es0108077, 2002. 10860

St. Clair, J. M., McCabe, D. C., Crounse, J. D., Steiner, U., and Wennberg, P. O.: Chemical ionization tandem mass spectrometer for the in situ measurement of methyl hydrogen peroxide, Rev. Sci. Instrum., 81, 094102, doi:10.1063/1.3480552, 2010. 10863

Tkacik, D. S., Presto, A. A., Donahue, N. M., and Robinson, A. L.: Secondary organic aerosol formation from intermediate-volatility organic compounds: cyclic, linear, and branched alkanes, Environ. Sci. Technol., 46, 8773–8781, doi:10.1021/es301112c, 2012. 10861

Van Krevelen, D. W.: Graphical-statistical method for the study of structure and reaction processes of coal, Fuel, 24, 269–284, 1950. 10876

Yee, L. D., Craven, J. S., Loza, C. L., Schilling, K. A., Ng, N. L., Canagaratna, M. R., Ziemann, P. J., Flagan, R. C., and Seinfeld, J. H.: Secondary organic aerosol formation from low-NO$_x$ photooxidation of dodecane: evolution of multigeneration gas-phase chemistry and aerosol composition, J. Phys. Chem. A, 116, 6211–6230, doi:10.1021/jp211531h, 2012. 10861, 10862, 10864, 10865, 10867, 10869, 10871, 10877

Title Page

Abstract | Introduction

Conclusions | References

Tables | Figures

|◀ | ▶|

◀ | ▶

Back | Close

Full Screen / Esc

Printer-friendly Version

Interactive Discussion

Zhang, X. and Seinfeld, J. H.: A Functional Group Oxidation Model (FGOM) for SOA formation and aging, Atmos. Chem. Phys. Discuss., 12, 32565–32611, doi:10.5194/acpd-12-32565-2012, 2012. 10861

Ziemann, P. J.: Formation of alkoxyhydroperoxy aldehydes and cyclic peroxyhemiacetals from reactions of cyclic alkenes with O_3 in the presence of alcohols, J. Phys. Chem. A, 107, 2048–2060, doi:10.1021/jp022114y, 2003. 10874

Effect of chemical structure on SOA formation

L. D. Yee et al.

Title Page

Abstract | Introduction

Conclusions | References

Tables | Figures

|◄ | ►|

◄ | ►

Back | Close

Full Screen / Esc

Printer-friendly Version

Interactive Discussion

ACPD

13, 10859–10903, 2013

Effect of chemical structure on SOA formation

L. D. Yee et al.

Title Page

Abstract | Introduction

Conclusions | References

Tables | Figures

◄ | ►►

◄ | ►

Back | Close

Full Screen / Esc

Printer-friendly Version

Interactive Discussion

Table 1. C_{12} compounds studied.

Compound	Structure	V.P.[a] @ 25°C (atm)	$k_{OH} \times 10^{12}$[b] (molec cm^{-3} s^{-1})
n-dodecane		2.59×10^{-4}	13.9
2-methylundecane		4.1×10^{-4}	13.1
hexylcyclohexane		2.59×10^{-4}	17.4
cyclododecane		1.64×10^{-4}	14.7

[a] Using EVAPORATION (Compernolle et al., 2011)
[b] Calculated using relative rate from *n*-dodecane k_{OH} in MCM (Jenkin et al., 1997).

Table 2. Experimental conditions.

Expt	Organic	Duration of photooxidation (h)	Initial HC (ppb$_v$)	[NO]$_0$ (ppb$_v$)	[NO$_x$]$_0$ (ppb$_v$)	[O$_3$]$_0$ (ppb$_v$)	Initial Seed Vol. μm^3 cm^{-3}	Δ HC (ppb$_v$)	Peak Organic[a] μg m^{-3}
1	*n*-dodecane	18	33.0	< LDL[b]	< LDL[b]	3.3	12.0	32.3	51.3
2	*n*-dodecane	36	34.9	< LDL[b]	< LDL[b]	2.6	11.4	33.6	62.8
3	2-methylundecane	18	27.3	< LDL[b]	< LDL[b]	4.0	16.3	22.4	not available[c]
4	2-methylundecane	36	28.9	< LDL[b]	< LDL[b]	4.2	13.6	27.6	45.6
5	hexylcyclohexane	18	16.2	< LDL[b]	< LDL[b]	2.4	10.5	15.2	34.8
6	hexylcyclohexane	36	14.9	< LDL[b]	< LDL[b]	3.8	4.2	14.4	34.4
7	cyclododecane	18	10.1	< LDL[b]	< LDL[b]	2.0	24.4	9.2	19.5[d]
8	cyclododecane	36	11.0	< LDL[b]	< LDL[b]	3.1	14.1	10.6	30.8

[a] Not corrected for particle wall loss
[b] Below lower detection limit (5 ppb$_v$)
[c] AMS not sampling
[d] Reported for end of experiment, though growth had not peaked.

Table 3. Selected ions monitored by the CIMS for *n*-dodecane and 2-methylundecane.

Mode	Observed *m/z*	Chemical Formula	Assignment
(−)	287	$C_{12}H_{26}O_2$	ROOH
(+)	223	$C_{12}H_{24}O$	CARB
(+)	204	$C_{12}H_{24}O_3$	CARBROOH
(−)	285	$C_{12}H_{24}O_2$	OHCARB
(−)	135/201	$C_6H_{12}O_2$	C6CARBACID

Table 4. Selected ions monitored by the CIMS for hexylcyclohexane and cyclododecane.

Mode	Observed m/z	Chemical Formula	Assignment
(−)	285	$C_{12}H_{24}O_2$	ROOH
(+)	221	$C_{12}H_{22}O$	CARB
(−)	299	$C_{12}H_{22}O_3$	CARBROOH
(−)	283	$C_{12}H_{22}O_2$	OHCARB
(−)	135/201	$C_6H_{12}O_2$	C6CARBACID

Table 5. Selected ions monitored by the AMS in the *n*-dodecane and 2-methylundecane systems.

Observed *m/z*	Exact mass ion formula	Proposed assignment
183	$C_{12}H_{23}O^+$	CARBROOH + CARBROOH PHA
215	$C_{12}H_{23}O_3^+$	CARBROOH PHA
185	$C_{12}H_{25}O^+$	OHROOH + OHROOH PHA
217	$C_{12}H_{25}O_3^+$	OHROOH PHA
197	$C_{12}H_{21}O_2^+$	DICARBROOH + DICARBROOH PHA
229	$C_{12}H_{21}O_4^+$	DICARBROOH PHA + CYC. OHDICARBROOH
199	$C_{12}H_{23}O_2^+$	OHCARBROOH + OHCARBROOH PHA
231	$C_{12}H_{23}O_4^+$	OHCARBROOH PHA
201	$C_{12}H_{25}O_2^+$	DIROOH
211	$C_{12}H_{19}O_3^+$	TRICARBROOH + TRICARBROOH PHA
243	$C_{12}H_{19}O_5^+$	TRICARBROOH PHA
213	$C_{12}H_{21}O_3^+$	OHDICARBROOH + OHDICARBROOH PHA
245	$C_{12}H_{21}O_5^+$	OHDICARBROOH PHA

Title Page

Abstract | Introduction

Conclusions | References

Tables | Figures

Back | Close

Full Screen / Esc

Printer-friendly Version

Interactive Discussion

Table 6. Selected ions monitored by the AMS in the hexylcyclohexane system.

Observed *m/z*	Exact mass ion formula	Proposed assignment
179	$C_{12}H_{19}O^+$	OHCARBROOH DHF
181	$C_{12}H_{21}O^+$	CARBROOH + CARBROOH PHA
213	$C_{12}H_{21}O_3^+$	CARBROOH PHA
183	$C_{12}H_{23}O^+$	OHROOH + OHROOH PHA
215	$C_{12}H_{23}O_3^+$	OHROOH PHA
195	$C_{12}H_{19}O_2^+$	DICARBROOH + DICARBROOH PHA
227	$C_{12}H_{19}O_4^+$	DICARBROOH PHA + CYC. OHDICARBROOH
197	$C_{12}H_{21}O_2^+$	OHCARBROOH + OHCARBROOH PHA
229	$C_{12}H_{21}O_4^+$	OHCARBROOH PHA
199	$C_{12}H_{23}O_2^+$	DIROOH
209	$C_{12}H_{17}O_3^+$	TRICARBROOH + TRICARBROOH PHA
211	$C_{12}H_{19}O_3^+$	OHDICARBROOH + OHDICARBROOH PHA
243	$C_{12}H_{19}O_5^+$	OHDICARBROH PHA

Title Page

Abstract | Introduction

Conclusions | References

Tables | Figures

◀ | ▶

◀ | ▶

Back | Close

Full Screen / Esc

Printer-friendly Version

Interactive Discussion

Table 7. Selected ions monitored by the AMS in the cyclododecane system.

Observed *m/z*	Exact mass ion formula	Proposed assignment
181	$C_{12}H_{21}O^+$	CARBROOH + CARBROOH PHA
213	$C_{12}H_{21}O_3^+$	CARBROOH PHA
183	$C_{12}H_{23}O^+$	OHROOH + OHROOH PHA
215	$C_{12}H_{23}O_3^+$	OHROOH PHA
195	$C_{12}H_{19}O_2^+$	DICARBROOH + DICARBROOH PHA
227	$C_{12}H_{19}O_4^+$	DICARBROOH PHA
197	$C_{12}H_{21}O_2^+$	OHCARBROOH + OHCARBROOH PHA
229	$C_{12}H_{21}O_4^+$	OHCARBROOH PHA
199	$C_{12}H_{23}O_2^+$	DIROOH
207	$C_{12}H_{15}O_3^+$	OH4CARBROOH
223	$C_{12}H_{15}O_4^+$	CYC. OH4CARBROOH
209	$C_{12}H_{17}O_3^+$	TRICARBROOH/4CARBROOH Ring Opened
225	$C_{12}H_{17}O_4^+$	CYC. TRICARBROOH
211	$C_{12}H_{19}O_3^+$	OHDICARBROOH/TRICARBROOH Ring Opened
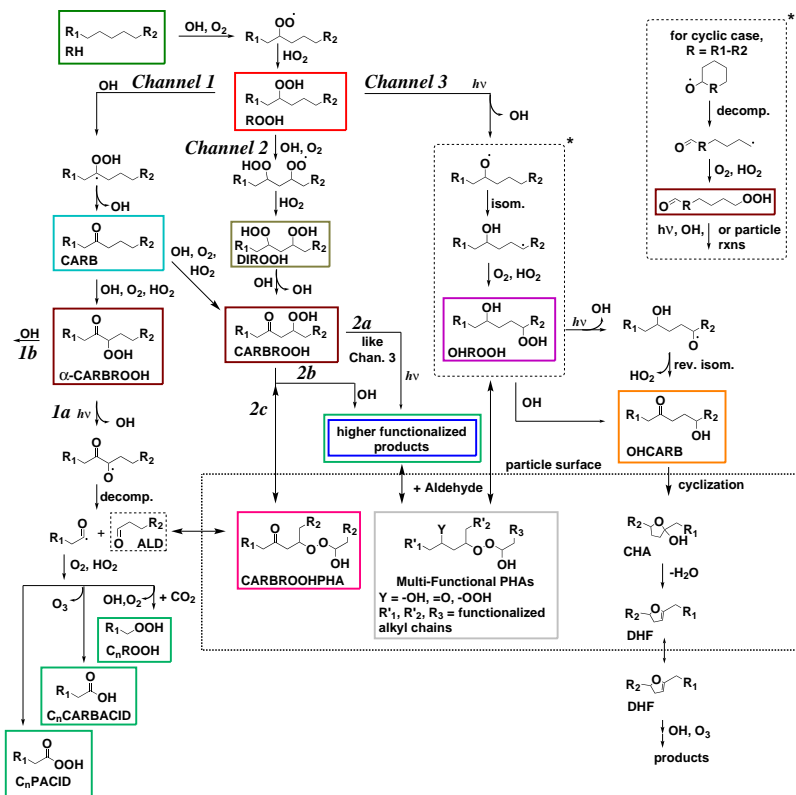
Fig. 1. General mechanism for alkanes under low-NO$_x$ conditions. R$_1$ and R$_2$ are alkyl groups. Solid boxed compounds indicate proposed structures monitored by the CIMS in the gas-phase and/or the AMS in the particle-phase. Pathway in upper right with asterisk denotes alternative pathway for the cyclic case (R$_1$ and R$_2$ are bonded together as R).
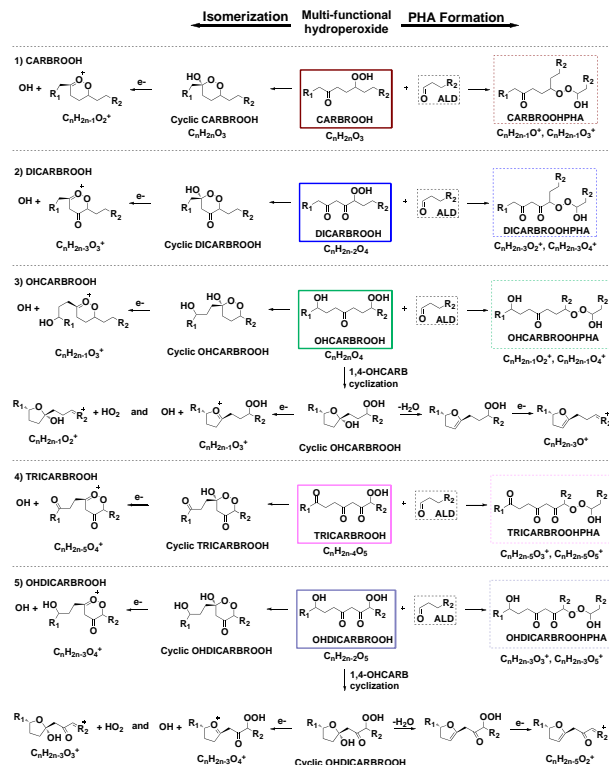
Fig. 2. General mechanism for particle-phase chemistry involving PHA formation (right-hand side) and potential isomerization (left-hand side) from higher functionalized products (solid boxed) formed along Channel 2 in Fig. 1. R_1 and R_2 are alkyl groups. One isomer shown. Dashed boxed compounds indicate PHA structures for which AMS ion tracers exist. General chemical and ion formulae for multi-functional hydroperoxides and proposed PHA and isomerization products shown, where n=12. Analogous products for hexylcyclohexane and cyclodo-decane would have an additional degree of unsaturation.
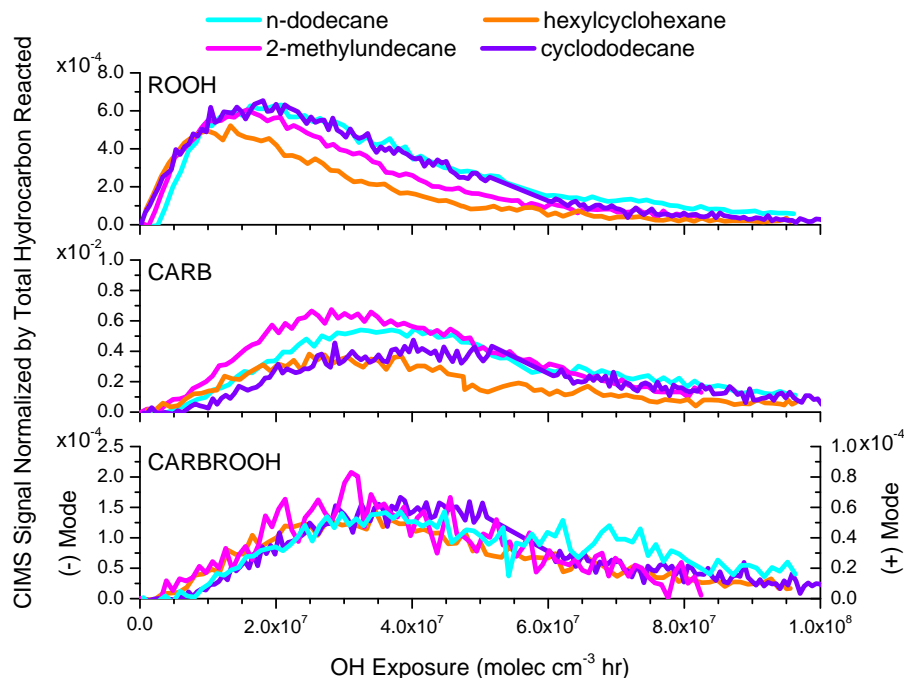
Fig. 3. Gas-phase trends of major species formed in the first three generations of photooxidation. Top panel: First-generation hydroperoxide (ROOH), Middle Panel: Second-generation carbonyl (CARB), and bottom panel: Third-generation carbonyl hydroperoxide (CARBROOH). Note that the CARBROOH was monitored in positive mode for *n*-dodecane and 2-methylundecane (the right side axis) and in negative mode for hexylcyclohexane and cyclododecane (the left side axis).
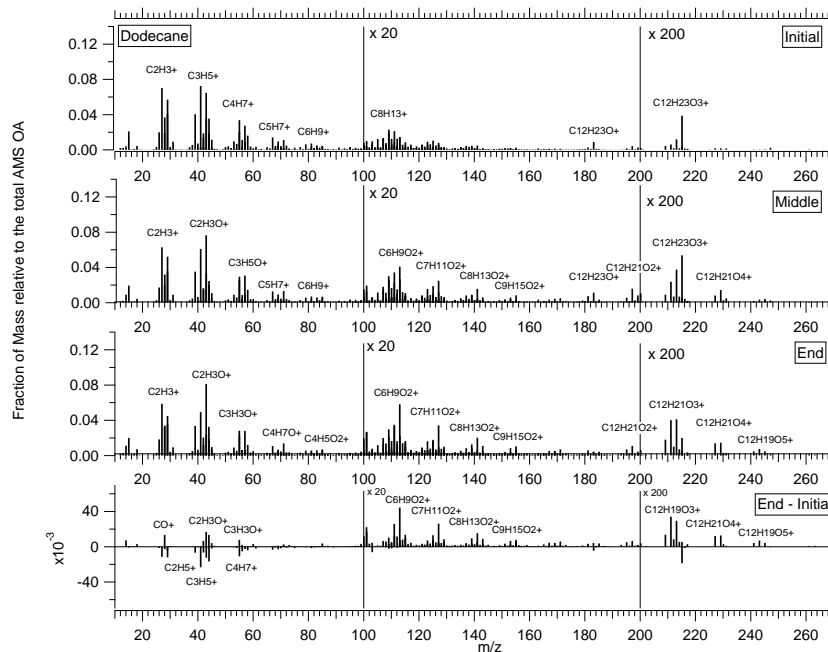
Fig. 4. High-resolution mass spectrum of SOA formed from *n*-dodecane at initial organic growth, mid-experiment, and end of experiment. The difference spectrum is also shown. *m/z*'s 101–200 are multiplied by 20, and *m/z*'s 201–300 are multiplied by 200 for visual clarity. Ions with high signal are labeled.

Title Page

Abstract | Introduction

Conclusions | References

Tables | Figures

|◄ | ►|

◄ | ►

Back | Close

Full Screen / Esc

Printer-friendly Version

Interactive Discussion

Discussion Paper | Discussion Paper | Discussion Paper | Discussion Paper

ACPD

13, 10859–10903, 2013

Effect of chemical structure on SOA formation

L. D. Yee et al.

Title Page

Abstract | Introduction

Conclusions | References

Tables | Figures

|◄ | ►|

◄ | ►

Back | Close

Full Screen / Esc

Printer-friendly Version

Interactive Discussion
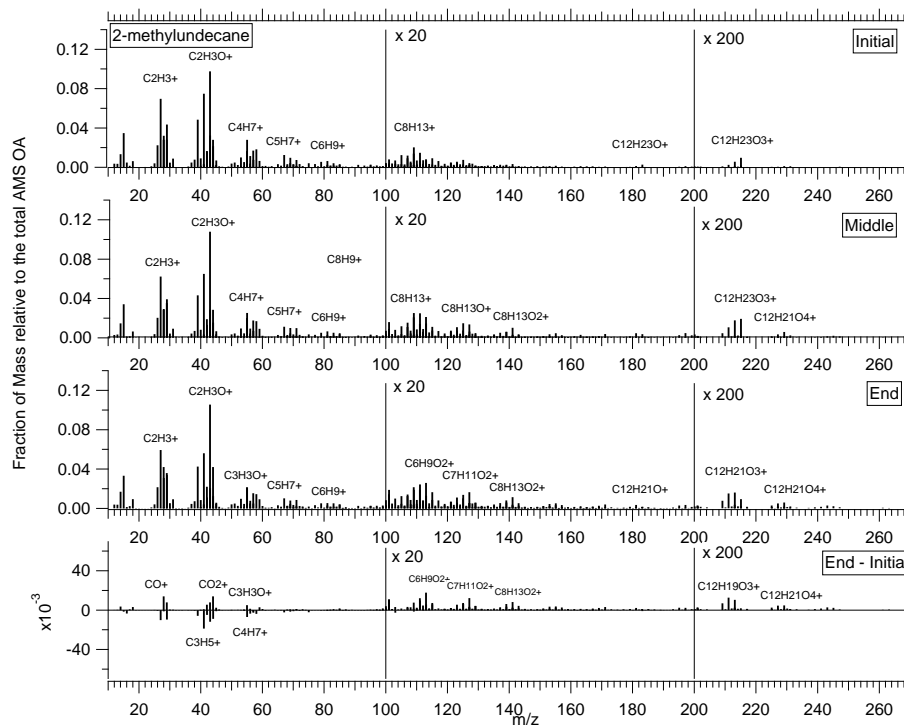
Fig. 5. High-resolution mass spectrum of SOA formed from 2-methylundecane at initial organic growth, mid-experiment, and end of experiment. The difference spectrum is also shown. *m/z*'s 101–200 are multiplied by 20, and *m/z*'s 201–300 are multiplied by 200 for visual clarity. Ions with high signal are labeled.
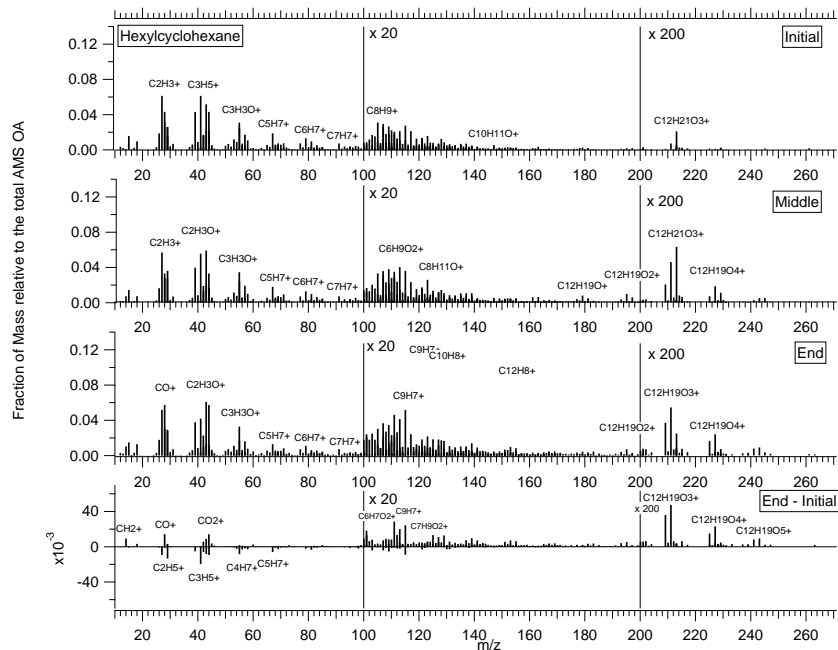
Fig. 6. High-resolution mass spectrum of SOA formed from hexylcyclohexane at initial organic growth, mid-experiment, and end of experiment. The difference spectrum is also shown. *m/z*'s 101–200 are multiplied by 20, and *m/z*'s 201–300 are multiplied by 200 for visual clarity. Ions with high signal are labeled.
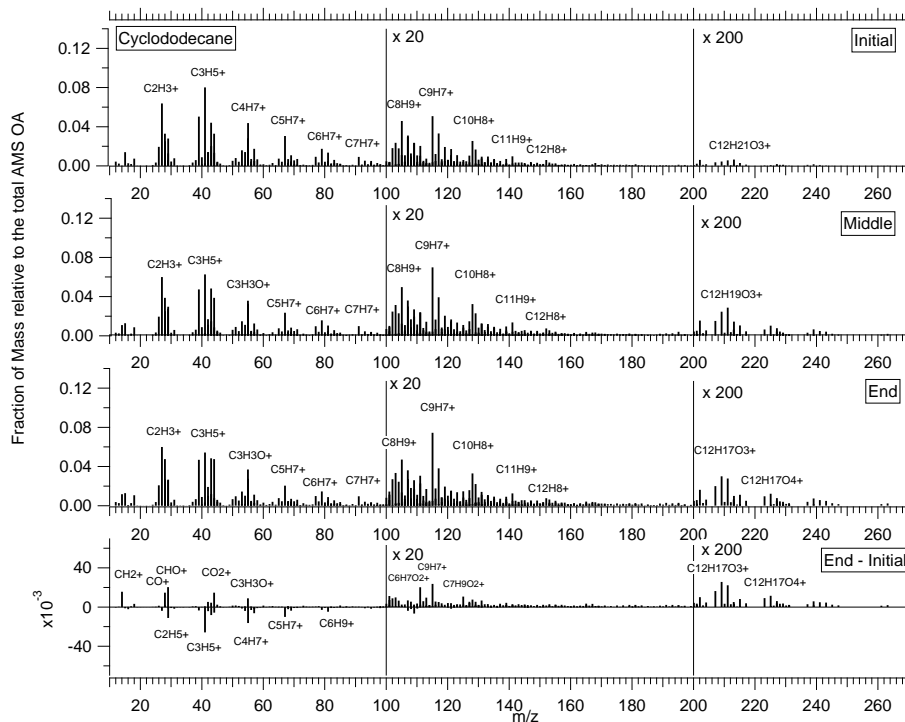
Fig. 7. High-resolution mass spectrum of SOA formed from cyclododecane at initial organic growth, mid-experiment, and end of experiment. The difference spectrum is also shown. *m/z*'s 101–200 are multiplied by 20, and *m/z*'s 201–300 are multiplied by 200 for visual clarity. Ions with high signal are labeled.

Title Page

Abstract   Introduction

Conclusions   References

Tables   Figures

◀   ▶

◀   ▶

Back   Close

Full Screen / Esc

Printer-friendly Version

Interactive Discussion
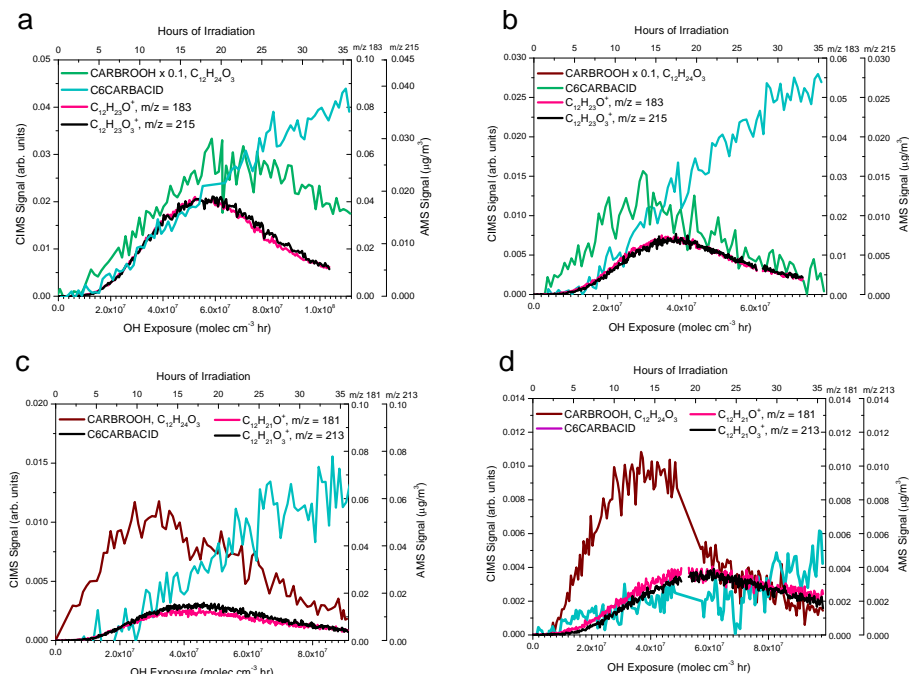
Fig. 8. Gas-phase trends of the **(a)** *n*-dodecane, **(b)** 2-methylundecane, **(c)** hexylcyclohexane, and **(d)** cyclododecane generated carbonyl hydroperoxide (CARBROOH) and C_6 carboxylic acid (C6CARBACID) as monitored by the CIMS and the CARBROOH and its derived PHA in the particle phase. CARBROOH and its PHA are tracked by AMS ions $C_{12}H_{23}O^+$ and $C_{12}H_{23}O_3^+$ for *n*-dodecane and 2-methylundecane, and by $C_{12}H_{21}O^+$ and $C_{12}H_{21}O_3^+$ for hexylcyclohexane and cylododecane.
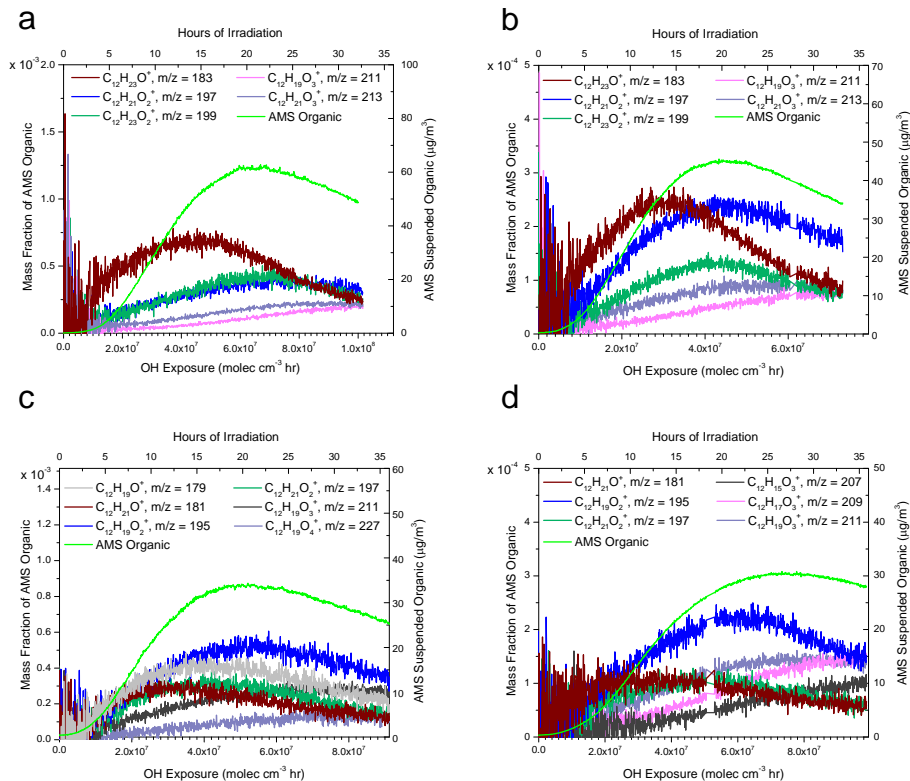
Fig. 9. Characteristic ions in **(a)** *n*-dodecane, **(b)** 2-methylundecane, **(c)** hexylcyclohexane, and **(d)** cyclododecane aerosol measured by the AMS.

Effect of chemical structure on SOA formation

L. D. Yee et al.

Title Page

Abstract | Introduction

Conclusions | References

Tables | Figures

◄ | ►►

◄ | ►

Back | Close

Full Screen / Esc

Printer-friendly Version

Interactive Discussion
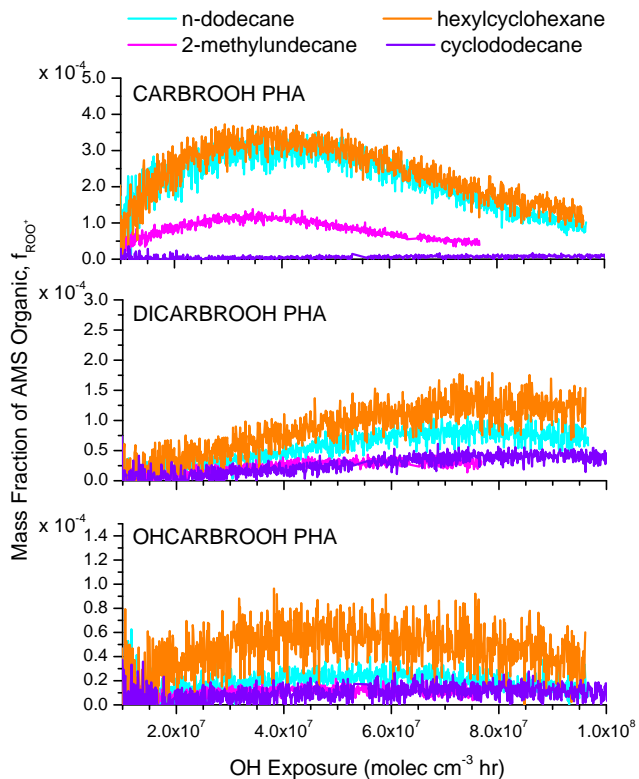
Fig. 10. Fraction of organic attributed to the corresponding ROO^+ PHA tracer ion for (top) carbonyl hyderoperoxide PHA (CARBROOH PHA), (middle) dicarbonyl hydroperoxide (DICARBROOH), and (bottom) hydroxycarbonyl hydroperoxide (OHCARBROOH).
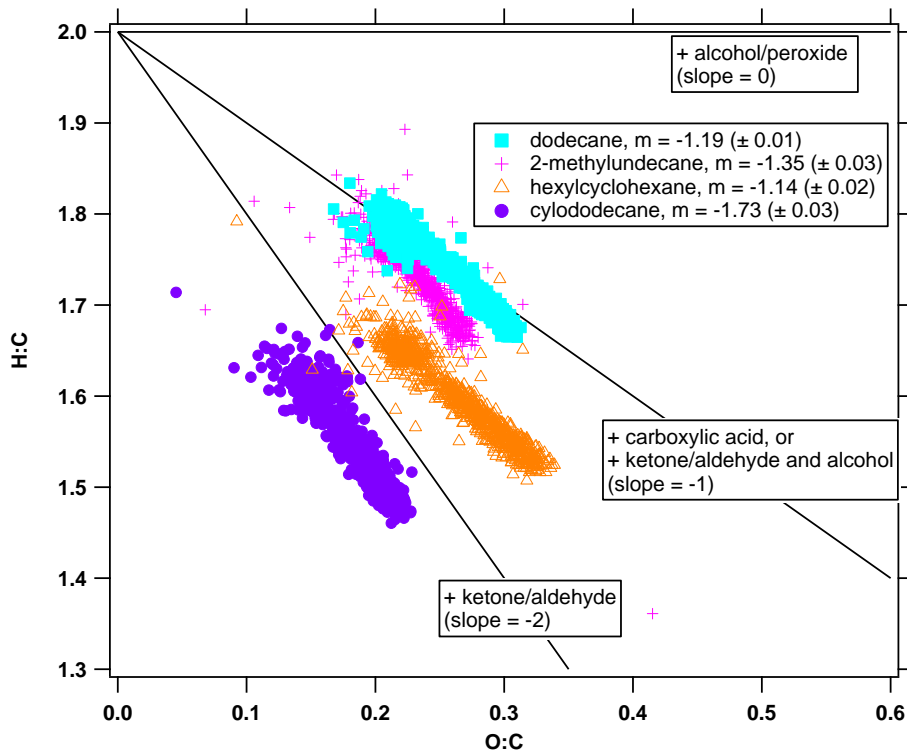
Fig. 11. Van Krevelen diagram for low-NO$_x$ photooxidation of *n*-dodecane, 2-methylundecane, hexylcyclohexane, and cyclododecane.

Legend from figure:
- dodecane, m = -1.19 (± 0.01)
- 2-methylundecane, m = -1.35 (± 0.03)
- hexylcyclohexane, m = -1.14 (± 0.02)
- cylododecane, m = -1.73 (± 0.03)

+ alcohol/peroxide (slope = 0)

+ carboxylic acid, or + ketone/aldehyde and alcohol (slope = -1)

+ ketone/aldehyde (slope = -2)